ChemComm

COMMUNICATION

View Article Online
View Journal

Cite this: DOI: 10.1039/d6cc01739h

Received 23rd March 2026,
Accepted 10th May 2026

DOI: 10.1039/d6cc01739h

rsc.li/chemcomm

Arrested mesoscopic growth of toroidal nanoobjects by molecular control of interaction surfaces

Ryuichi Kawai,[a] Yuhei Yamada,[a] Sougata Datta,[b] Hiroki Hanayama[c] and Shiki Yagai *[bc]

We show that hierarchical self-assembly at the mesoscale can be programmed by controlling the interaction surfaces of toroidal nanoobjects. Unlike analogous systems that undergo continuous higher-order growth into nanotubes, these toroids undergo selective dimerization in solution upon concentration but are prevented from further elongation into nanotubes.

In molecule-based supramolecular assemblies at the nanoscale, the number and steric arrangement of interactive sites can be programmed through rational molecular design and sophisticated organic synthesis, enabling the rational control over whether molecules can form discrete or polymeric assemblies.[1–16] Applying the same logic to hierarchical assemblies, in which primary supramolecular assemblies further organize into higher-order mesoscopic structures, is considerably more difficult because nanoscale building blocks that present well-defined interaction surfaces are not straightforward to design. If those surfaces could be encoded by supramolecular design, the assemblies themselves could be treated as "mesoscopic molecules", and their higher-order self-assembly might become programmable.[3,17–21] Realizing this possibility would extend the design principles of supramolecular polymerization and self-assembly into the mesoscale regime by treating organized supramolecular assemblies as intermediate hierarchical units, analogous to supramolecular polymerization observed in proteins.

We previously reported a scissor-shaped 9,10-diphenylanthracene dyad **1**,[22] which undergoes highly cooperative self-assembly to form nanotubes (Fig. 1a). In a nonpolar solvent, dyad **1** adopts a wedge-shaped, intramolecularly folded conformation stabilized by hydrogen bonding and π–π interactions, and the intermolecular association of these folded dyads gives rise to tubular assemblies (Fig. 1b). These tubes elongate into long, highly ordered structures through continuous intermolecular interactions between anthracene chromophores. All-atom molecular dynamics (AA-MD) simulations of **1** revealed that the tubular structure can be described as a stack of annular layers composed of radially arranged anthracene units. Anthracene moieties projecting from both sides of the folded monomer mediate interlayer interactions, which drive continuous layer-by-layer stacking along the tube axis. Accordingly, this persistent interlayer stacking results in the formation of highly ordered tubular structures. Based on these findings, we hypothesized that controlling this interlayer stacking process would allow the growth to be arrested at lower-order states, such as toroids.

Guided by this hypothesis, we designed and synthesized scissor-shaped 1,4-diphenylanthracene dyad **2**, in which the substitution pattern of the anthracene units was shifted to the 1,4-positions (Fig. 1a). In **2**, the 1,4-diphenylanthracene units project from only one side of the folded structure and are therefore expected to weaken interlayer contacts between adjacent annular layers. In a nonpolar solvent, **2** self-assembled into a mixture of toroids and fibrous precipitates, presumably because conformational isomerism of the folded molecules provides an alternative pathway for extended self-assembly. The soluble toroids were observed both as isolated species and as stacked dimers. Upon concentration of a purified toroid solution, the fraction of stacked dimers increased, whereas higher-order stacks beyond trimers were rarely observed. These results demonstrate that molecular design can regulate the hierarchical elongation of nanoscale objects into mesoscopic assemblies.

Because dyad **2** (for the synthesis and characterization, see SI) was soluble in toluene but only sparingly soluble in methylcyclohexane (MCH), the self-assembly of **2** in MCH containing 10% toluene (v/v) at c = 100 μM was investigated by variable-temperature UV/Vis absorption spectroscopy. At 100 °C, **2**

[a] Division of Advanced Science and Engineering, Graduate School of Engineering, Chiba University, 1-33 Yayoi-cho, Inage-ku, Chiba 263-8522, Japan
[b] Institute for Advanced Academic Research (IAAR), Chiba University, 1-33 Yayoi-cho, Inage-ku, Chiba 263-8522, Japan. E-mail: yagai@faculty.chiba-u.jp
[c] Department of Applied Chemistry and Biotechnology, Graduate School of Engineering, Chiba University, 1-33 Yayoi-cho, Inage-ku, Chiba 263-8522, Japan

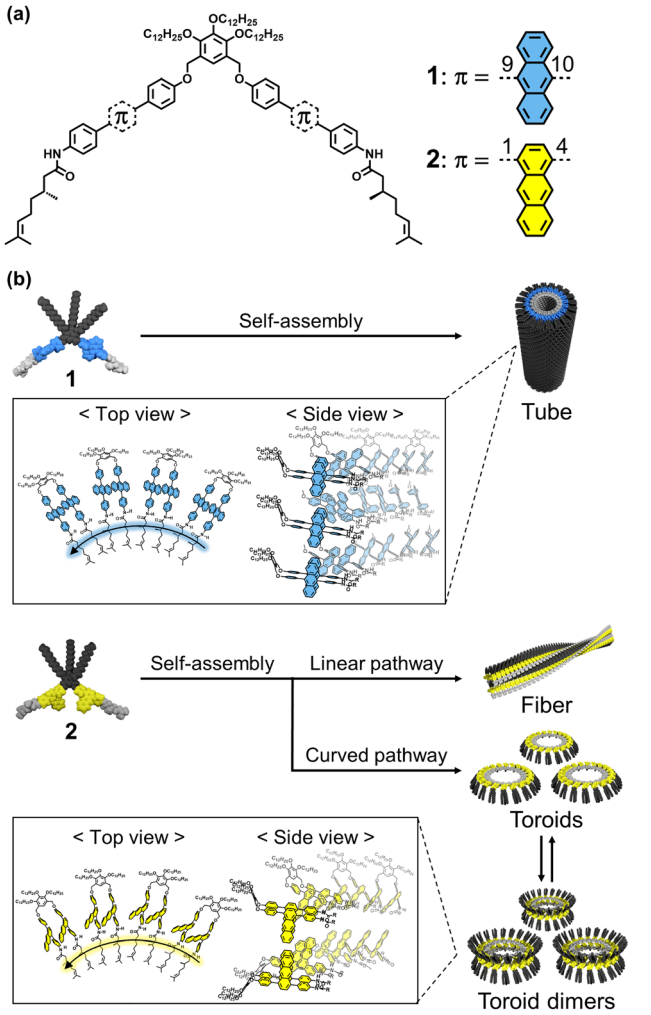

Fig. 1 (a) Molecular structures of **1** and **2**. (b) Schematic representations of self-assembly processes of **1** and **2**.

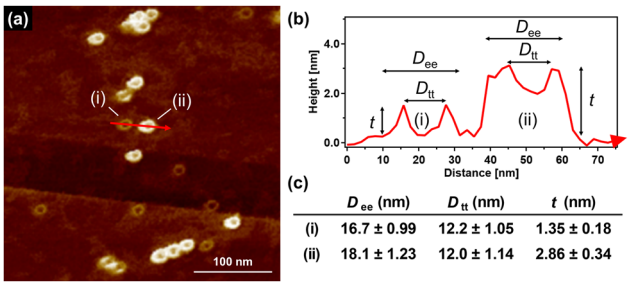

	D_{ee} (nm)	D_{tt} (nm)	t (nm)
(i)	16.7 ± 0.99	12.2 ± 1.05	1.35 ± 0.18
(ii)	18.1 ± 1.23	12.0 ± 1.14	2.86 ± 0.34

Fig. 2 (a) AFM image of toroids of **2** (c = 100 μM) prepared by spin-coating an MCH solution containing 10% (v/v) toluene immediately after cooling from 100 °C to 0 °C at a rate of 1 °C min^{-1}. (b) AFM cross-sectional analysis of toroids along the red arrow in (a). (c) Average edge-to-edge diameter (D_{ee}), top-to-top diameter (D_{tt}) and thickness (t) values calculated by analysing 100 toroids in AFM images.

displayed vibronic bands in the range of 354–393 nm, which are characteristic of the π–π* transition of anthracene chromophores (Fig. S1a, red line). Upon cooling the hot monomeric solution to 0 °C at a rate of 1 °C min^{-1} under the same conditions as those for dyad **1**,[22] the absorption maxima bathochromically shifted from 375 and 393 nm to 388 and 408 nm (Fig. S1a, blue line), respectively, indicating J-type stacking of the anthracene chromophores. After cooling, precipitation was visually apparent in the solution (Fig. S1b). Atomic force microscopy (AFM) imaging of the precipitate, spin-coated onto highly oriented pyrolytic graphite (HOPG), revealed bundled fibers with an apparent width of approximately 50 nm (Fig. S1c). AFM cross-sectional analysis showed that the width of the elementary fibrils constituting the fibers was approximately 7 nm (Fig. S1d), corresponding to the molecular length of the folded monomer **2**. The FT-IR spectra of the fibers suggested the involvement of amide hydrogen bonding (Fig. S2, yellow dotted line).

Interestingly, AFM observation of the supernatant revealed that **2** forms two types of toroids with clearly distinct thicknesses (*e.g.*, i and ii in Fig. 2a). Cross-sectional analysis revealed that the edge-to-edge diameter (D_{ee}) and top-to-top diameter (D_{tt}) of these toroids were approximately 17–18 nm and 12 nm, respectively (Fig. 2b and c), consistent with those of our previously reported toroids.[17,22–25] The thickness (t) was estimated to be 1.4 nm for thinner toroids and 2.9 nm for thicker toroids, respectively, indicating that the thicker toroid corresponds to the dimeric form of the thinner toroid. To quantify the molar distribution of **2** between fibers and toroids, the toroids were purified by passing the entire suspension through a membrane filter with a pore size of 200 nm (Fig. S3a and b).[25,26] The total concentration of monomer in the filtrate was estimated to be *ca.* 15 μM from the UV/Vis absorption spectrum, indicating that *ca.* 15% of **2** followed the curved pathway to form toroids (Fig. S3c). In the FT-IR spectra, the N–H and C=O stretching vibration bands of the amide groups exhibited larger shifts for the toroids than for the fibers, suggesting stronger amide hydrogen-bonding interactions in the toroids (Fig. S2, yellow solid line).

To gain insight into the supramolecular polymorphism of **2**, we considered two possible intramolecularly folded conformations: parallel and anti-parallel conformations. We thus performed all-atom molecular dynamics (AA-MD) simulations of linear decameric stacks of **2** with the two conformations. Production MD simulations for 110 ns (see the SI for details) showed that stacks composed of the parallel conformer underwent fragmentation, whereas those composed of the anti-parallel conformer retained their linear structure (Fig. S4). This result suggests that the parallel conformer is unable to maintain extended linear structures.[27–29] Therefore, extended fibers are proposed to arise from self-assembly of the anti-parallel conformer, whereas toroids are proposed to arise from self-assembly of the parallel conformer.

We found that the toroids formed by **2** underwent dimerization upon concentration of the above solution. Analysis of toroid counts in AFM images revealed that 47% of the toroids were already present in the dimeric form at c = 15 μM (Fig. 3a and b; for details, see SI). Concentrating this solution under an N_2 flow increased the fraction of dimerized toroids to 85% at c = 120 μM (Fig. 3a–c, S5a–h and Table S2). The fraction of toroids that further stacked into oligomeric species larger than trimers remained below 2% at c = 120 μM. This behavior is

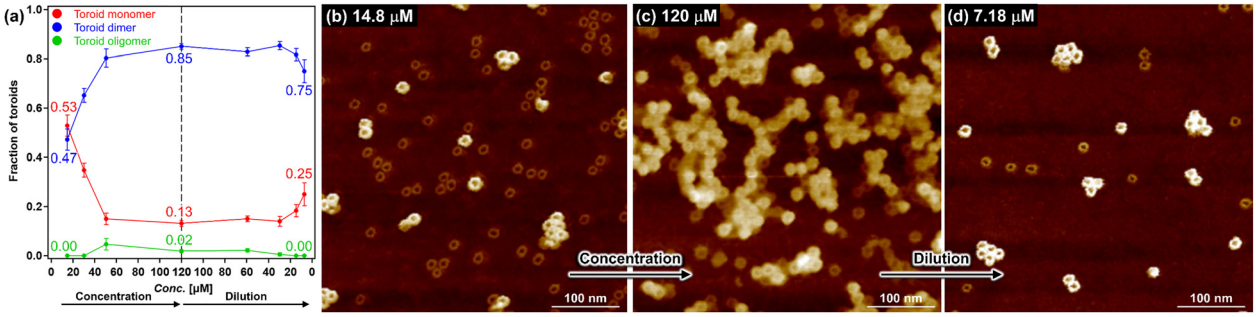

Fig. 3 (a) Plots of the fraction of dimerized toroids as a function of concentration of **2** during both concentration and subsequent dilution. (b)–(d) AFM images of toroids at (b) 14.8 μM and (c) 120 μM, respectively, during concentration, and at (d) 7.18 μM during subsequent dilution.

reminiscent of anti-cooperative supramolecular polymerization observed in molecular π-stacking systems,[2,4,16,30–32] and can be attributed to the parallel conformation of folded **2** in the toroid (Fig. 1b). In this conformation, the anthracene moieties project from only one side of the toroid, such that the sites involved in inter-toroid interactions are limited to a single face. Therefore, these interaction sites are likely saturated upon dimer formation.

Interestingly, upon dilution of the above concentrated solution to c = 7 μM, corresponding to approximately half of the initial concentration, the fraction of dimerized toroids remained high at 75% (Fig. 3a, d, Fig. S5i–p and Table S2). This finding suggests hysteresis between the concentration-induced dimerization and dilution-induced dissociation processes. Even after aging the diluted solution for 8 days, the fraction of dimerized toroids decreased only slightly, from 65% to 55% (c = 4.90 μM), indicating the kinetic stability of the toroid dimer. Throughout these dimerization and dissociation processes, the UV/Vis absorption, circular dichroism (CD) and fluorescence spectra remained essentially unchanged (Fig. S6). These results suggest that interactions between the anthracene moieties projecting from one side of the toroids are not individually strong or specific enough to give rise to appreciable excitonic coupling or excimer formation.[33] Thus, the toroid dimers are stabilized by the cumulative effect of multipoint interactions distributed around the entire circumference of the toroid.

To further verify the presence of toroid dimers in solution, we performed *in situ* small-angle X-ray scattering (SAXS) measurements. The scattering profiles of the toroid dimer solution (c = 305 μM) were well fitted by a hollow-cylinder model consisting of a solvent core and three concentric shells corresponding to the branched alkyl chains, the aromatic region and n-$C_{12}H_{25}$ chains, respectively (Fig. 4a, b and Table S1). The fitted parameters indicated a toroidal (tubular) structure with a thickness of 5.2 nm, and inner and outer diameters of approximately 7 and 16 nm, respectively, which were consistent with AFM observations. In contrast, the thickness was larger than that estimated by AFM analysis (2.9 nm), likely reflecting the difference between the solvated structure in solution and the partially collapsed structure observed under dry AFM conditions. Notably, a scattering peak corresponding to a spacing of 2.7 nm, which is half of the thickness, was also observed at

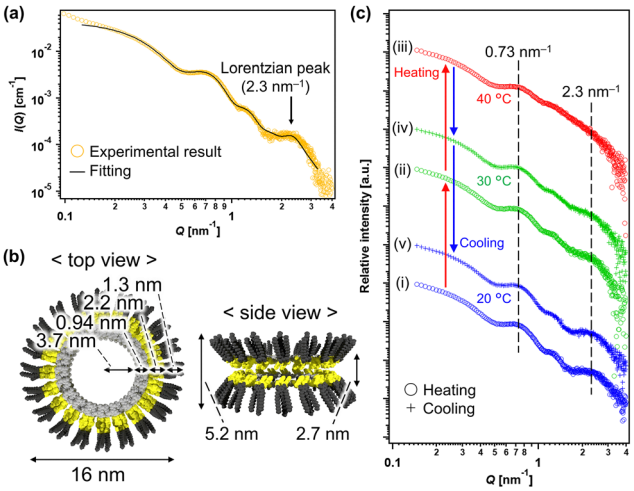

Fig. 4 (a) SAXS profiles of toroids of **2** (c = 305 μM) in MCH containing 10% (v/v) toluene. The scattering data was fitted using a modified core-multishell cylinder model with an additional Lorentzian peak at Q = 2.3 nm^{-1} corresponding to stacking of two toroids (black line). (b) Schematic illustrations of a toroid dimer of **2**. (c) Variable-temperature SAXS profiles of toroids of **2** (c = 242 μM) acquired during heating to 40 °C and subsequent cooling to 20 °C.

Q = 2.3 nm^{-1}. This observation clearly indicates the presence of a bilayer structure arising from the stacking of two toroids (Fig. 4b). This interpretation was further supported by variable-temperature *in situ* SAXS measurements. Upon heating the toroid dimer solution (c = 242 μM) to 40 °C, the scattering peak at Q = 2.3 nm^{-1} disappeared, while the scattering peak at Q = 0.73 nm^{-1}, corresponding to the diameter of the toroid, remained unchanged (Fig. 4c, profiles i to iii). This change indicates thermal dissociation of the toroid dimers into toroid monomers at 40 °C. Cooling the solution back to 20 °C restored the peak at Q = 2.3 nm^{-1} (Fig. 4c, profiles iii to v), reproducing the original SAXS profiles and demonstrating reversible reformation of the toroid dimers.

In conclusion, this work demonstrates that the design principles established for molecule-based supramolecular assemblies at the nanoscale can be extended to hierarchical assemblies at the mesoscale. By treating toroidal nanoobjects as mesoscopic molecules and restricting their available

interaction surface to a single face, we arrested hierarchical elongation into tubular architectures at the level of stacked dimers by saturating the available interaction sites. This arrested mesoscopic growth was directly visualized by AFM and corroborated by SAXS analysis. These findings establish a design principle for controlling hierarchical self-assembly in the mesoscopic regime and provide a foundation for mesoscale chemistry based on programmable nanoobjects.

S. Y. and R. K. designed the project. R. K. and Y. Y. performed all the experimental work. S. Y. and R. K. prepared the overall manuscript, including figures. All authors, including Y. Y., S. D., and H. H., contributed by commenting on the manuscript. S. Y. supervised the overall research.

Conflicts of interest

There are no conflicts to declare.

Data availability

The data that support the findings of this work have been included in the main text and supplementary information (SI). Supplementary information is available. See DOI: https://doi.org/10.1039/d6cc01739h.

Acknowledgements

This work was supported by the Japan Society for the Promotion of Science (JSPS) KAKENHI grant no. JP23H04873 in a Grant-in-Aid for Transformative Research Areas ''Materials Science of Meso-Hierarchy.'' This work was performed under the approval of the Photon Factory Program Advisory Committee (Proposal No. 2024G542). The authors are grateful to Dr Hideaki Takagi and Dr Rie Haruki for the SAXS measurements.

References

1 K. D. Shimizu and J. Rebek, *Proc. Natl. Acad. Sci. U. S. A.*, 1995, **92**, 12403–12407.
2 R. van der Weegen, P. A. Korevaar, P. Voudouris, I. K. Voets, T. F. A. de Greef, J. A. J. M. Vekemans and E. W. Meijer, *Chem. Commun.*, 2013, **49**, 5532–5534.
3 C. Rest, R. Kandanelli and G. Fernández, *Chem. Soc. Rev.*, 2015, **44**, 2543–2572.
4 J. Gershberg, F. Fennel, T. H. Rehm, S. Lochbrunner and F. Würthner, *Chem. Sci.*, 2016, **7**, 1729–1737.
5 K. Ohga, Y. Takashima, H. Takahashi, Y. Kawaguchi, H. Yamaguchi and A. Harada, *Macromolecules*, 2005, **38**, 5897–5904.
6 T. Seki, S. Yagai, T. Karatsu and A. Kitamura, *J. Org. Chem.*, 2008, **73**, 3328–3335.
7 R. S. Wilson-Kovacs, X. Fang, M. J. L. Hagemann, H. E. Symons and C. F. J. Faul, *Chem. – Eur. J.*, 2022, **28**, e202103443.
8 E. Lopez-Fontal, L. Milanesi and S. Tomas, *Chem. Sci.*, 2016, **7**, 4468–4475.
9 C. Kulkarni, E. W. Meijer and A. R. A. Palmans, *Acc. Chem. Res.*, 2017, **50**, 1928–1936.
10 T. Aida and E. W. Meijer, *Isr. J. Chem.*, 2020, **60**, 33–47.
11 R. Kudo, H. Hanayama, B. Vedhanarayanan, H. Tamiaki, N. Hara, S. E. Rogers, M. J. Hollamby, B. Manna, K. Harano and S. Yagai, *Org. Chem. Front.*, 2024, **11**, 6304–6310.
12 Y. Yamauchi, M. Yoshizawa, M. Akita and M. Fujita, *J. Am. Chem. Soc.*, 2010, **132**, 960–966.
13 F. Würthner and S. Yao, *Angew. Chem., Int. Ed.*, 2000, **39**, 1978–1981.
14 E. Kirchner, D. Bialas, F. Fennel, M. Grüne and F. Würthner, *J. Am. Chem. Soc.*, 2019, **141**, 7428–7438.
15 M. A. Niyas, K. Shoyama, M. Grüne and F. Würthner, *Nature*, 2025, **637**, 854–859.
16 C. Shao, M. Grüne, M. Stolte and F. Würthner, *Chem. – Eur. J.*, 2012, **18**, 13665–13677.
17 T. Saito, T. Kajitani and S. Yagai, *J. Am. Chem. Soc.*, 2023, **145**, 443–454.
18 K. Sugiyasu, *Polym. J.*, 2021, **53**, 865–875.
19 S. Datta, H. Itabashi, T. Saito and S. Yagai, *Nat. Chem.*, 2025, **17**, 477–492.
20 S. Datta, Y. Yamada, R. Kudo and S. Yagai, *Macromolecules*, 2026, **59**, 1069–1084.
21 Z. Geng, P. L.-Y. Chiu, M. H.-Y. Chan and V. W.-W. Yam, *Chemistry*, 2024, **10**, 1225–1239.
22 T. Aizawa, H. Arima, S. Mihara, T. Ueno, S. Yoshii, T. Saito, H. Itabashi, S. Datta, H. Hanayama, A. Sakamoto, R. Shimada, S. E. Rogers, M. J. Hollamby, T. Kajitani, Y. Ishii, G. Watanabe, K. Harano, T. Matsumoto, N. Pathoor, M. Vacha, H. Sotome and S. Yagai, *J. Am. Chem. Soc.*, 2026, **148**, 16894–16904.
23 S. Yagai, M. Yamauchi, A. Kobayashi, T. Karatsu, A. Kitamura, T. Ohba and Y. Kikkawa, *J. Am. Chem. Soc.*, 2012, **134**, 18205–18208.
24 J. S. Valera, H. Arima, C. Naranjo, T. Saito, N. Suda, R. Gómez, S. Yagai and L. Sánchez, *Angew. Chem., Int. Ed.*, 2022, **134**, e202114290.
25 N. Suda, T. Saito, H. Arima and S. Yagai, *Chem. Sci.*, 2022, **13**, 3249–3255.
26 A. Suzuki, K. Aratsu, S. Datta, N. Shimizu, H. Takagi, R. Haruki, S. Adachi, M. Hollamby, F. Silly and S. Yagai, *J. Am. Chem. Soc.*, 2019, **141**, 13196–13202.
27 K. Tashiro, T. Saito, H. Arima, N. Suda, B. Vedhanarayanan and S. Yagai, *Chem. Rec.*, 2022, **22**, e202100252.
28 N. Suda, H. Arima, T. Saito, T. Aizawa and S. Yagai, *Chem. Lett.*, 2022, **51**, 700–703.
29 T. Saito, D. Inoue, Y. Kitamoto, H. Hanayama, T. Fujita, Y. Watanabe, M. Suda, T. Hirose, T. Kajitani and S. Yagai, *Nat. Nanotechnol.*, 2025, **20**, 825–834.
30 K. Cai, J. Xie, D. Zhang, W. Shi, Q. Yan and D. Zhao, *J. Am. Chem. Soc.*, 2018, **140**, 5764–5773.
31 L. Herkert, J. Droste, K. K. Kartha, P. A. Korevaar, T. F. A. de Greef, M. R. Hansen and G. Fernández, *Angew. Chem., Int. Ed.*, 2019, **58**, 11344–11349.
32 I. Helmers, M. S. Hossain, N. Bäumer, P. Wesarg, B. Soberats, L. S. Shimizu and G. Fernández, *Angew. Chem., Int. Ed.*, 2022, **61**, e202200390.
33 F. Kannen, T. Adachi, M. Nishimura, K. Yoza and T. Kusukawa, *Molecules*, 2024, **29**, 407.

